J|A|C|S
ARTICLES
Published on Web 10/09/2004

Covalently Bonded $^{1}_{\infty}[Pt]^{-}$ Chains in BaPt: Extension of the Zintl−Klemm Concept to Anionic Transition Metals?

Andrey Karpov, Jürgen Nuss, Ulrich Wedig, and Martin Jansen*

Contribution from the Max-Planck-Institut für Festkörperforschung, Heisenbergstrasse 1, D-70569 Stuttgart, Germany

Received April 23, 2004; E-mail: m.jansen@fkf.mpg.de

Abstract: BaPt has been synthesized by reaction of a 1:1 mixture of Ba and Pt at 1223 K in argon and characterized by single-crystal X-ray structure determination and electrical resistivity and magnetic susceptibility measurements. The compound crystallizes in the NiAs structure type with an extremely low value for the *c*/*a* ratio (hexagonal space group $P6_3/mmc$ with $a = 5.057(2)$ Å, $c = 5.420(3)$ Å, $c/a = 1.072$, $R1 = 0.0297$, $N_{hkl} = 93$). This *c*/*a* ratio reflects structural features that are unusual for the NiAs type: Pt is coordinated linearly by two other Pt atoms at a distance as short as 2.71 Å, thus forming a chain along [001] of homonuclearly bonded platinum. Band structure calculations and electron localization function analyses reveal a covalent character of Pt−Pt interactions along the *c* axis and two-dimensional metallic conductivity parallel to the *ab* plane. In terms of the Zintl−Klemm concept, in its most general sense, BaPt can be formulated as $(Ba^{2+})(^{1}_{\infty}[Pt]^{-})\cdot e^{-}$, and it can be considered a new example of platinide anions in the solid state.

Introduction

Among the classes of inorganic solids, the intermetallics are the ones that are least understood with respect to their bonding properties.[1] Unlike ionically or covalently bonded compounds, it is virtually impossible to apply simple heuristic concepts to reliably deduce compositions or structural features from the elements involved and from the valence electron concentration (VEC) per atom provided. Also, the simple Fermi liquid picture usually fails to properly explain even basic physical properties such as electrical conductivity and magnetic susceptibility. This is mainly due to the fact that some of the features that primarily determine the chemical bond, such as the degrees of valence electron transfer and localization, vary strongly and almost continuously with composition and the nature of the elements involved. Several fruitful concepts for classifying the rich empirical knowledge on intermetallic systems have been developed,[2] the most efficient ones being based on the degree of electron transfer, occurring in the course of phase formation. A particularly successful approach, having predictive potential with respect to probable stabilities of yet unknown phases, has been introduced by A. R. Miedema.[3] Also, the Zintl−Klemm concept has proven a strong tool for classifying and qualitatively predicting structural features.[4,5] In this approach, which had been developed for intermetallic phases exclusively consisting of main group elements, at the transition to ionic bonding, a complete transfer of the valence electrons from the more electropositive component to the more electronegative one is assumed. The anions thus generated form covalently bonded homoatomic networks obeying the $8 - N$ rule, this way saturating open shells. The issue of extending the Zintl−Klemm concept to transition metals has been addressed, previously, assuming the transition metals to act as the electropositive constituents.[6] However, the inverse combinations of electropositive main group elements and electronegative transition metals have not been considered, so far. Although no covalently bonded negatively charged homoatomic partial structures of transition metals seem to be known to date, it is not justified to disregard such a scenario

(1) (a) Schön, J. C. *Angew. Chem.* **1995**, *107*, 1183−1185; *Angew. Chem., Int. Ed. Engl.* **1995**, *34*, 1081−1083. (b) Allen, L. C.; Burdett, J. K. *Angew. Chem.* **1995**, *107*, 2157−2158; *Angew. Chem., Int. Ed. Engl.* **1995**, *34*, 2003−2004.

(2) (a) Hume−Rothery, W. *J. Inst. Met.* **1926**, *35*, 313−367. (b) Frank, F. C.; Kasper, J. S. *Acta Crystallogr.* **1959**, *12*, 483−499. (c) Laves, F. In *Intermetallic Compounds*; Westbrook, J. H., Ed.; Wiley: New York, 1967; pp 129−143. (d) Pearson, W. B. *The Crystal Chemistry and Physics of Metals and Alloys*; Wiley-Interscience: New York, 1972. (e) Pearson, W. B. *J. Less-Common Met.* **1985**, *109*, L3−L6. (f) Nesper, R. *Angew. Chem.* **1991**, *103*, 805−834; *Angew. Chem., Int. Ed. Engl.* **1991**, *30*, 789−817. (g) Villars, P. In *Intermetallic Compounds Principles and Practice*; Westbrook, J. H., Fleischer, R. L., Eds.; John Wiley & Sons: Chichester, U.K., 1994; Vol. 1, pp 227−275. (h) Miller G. J. *Eur. J. Inorg. Chem.* **1998**, *5*, 523−536.

(3) (a) Miedema, A. R.; de Boer, F. R.; de Châtel, P. F. *J. Phys. F* **1973**, *3*, 1558−1576. (b) Miedema, A. R. *J. Less-Common Met.* **1973**, *32*, 117−136. (c) de Boer, F. R.; Boom, R.; Mattens, W. C. M.; Miedema, A. R.; Niessen, A. K. In *Cohesion in Metals, Transition Metal Alloys*; de Boer, F. R., Pettifor, D. G., Eds.; Cohesion and Structure; North-Holland Physics Publishing: Amsterdam, 1988; Vol. 1.

(4) (a) Zintl, E.; Brauer, G. *Z. Phys. Chem. B* **1933**, *20*, 245−271. (b) Zintl, E. *Angew. Chem.* **1939**, *52*, 1−6. (c) Klemm, W. *Proc. Chem. Soc. London* **1958**, 329−341. (d) Klemm, W. In *Festkoerperprobleme*; Sauter, F., Ed.; Vieweg: Braunschweig, Germany, 1963; Vol. 3, pp 233−251.

(5) Selected reviews: (a) Schäfer, H.; Eisenmann, B.; Müller, W. *Angew. Chem.* **1973**, *85*, 742−760; *Angew. Chem., Int. Ed. Engl.* **1973**, *12*, 694−712. (b) von Schnering, H. G. *Angew. Chem.* **1981**, *93*, 44−63; *Angew. Chem., Int. Ed. Engl.* **1981**, *20*, 33−51. (c) von Schnering, H. G. *Vortr.-Rheinisch-Westfael. Akad. Wiss., Nat.-, Ing.- Wirtschaftswiss.* **1984**, *325*, 7−30. (d) Corbett, J. D. *Chem. Rev.* **1985**, *85*, 383−397. (e) Nesper, R. *Prog. Solid State Chem.* **1990**, *20*, 1−45. (f) Corbett, J. D. *Angew. Chem.* **2000**, *112*, 682−704; *Angew. Chem., Int. Ed.* **2000**, *39*, 670−690.

(6) (a) *Chemistry, Structure and Bonding of Zintl Phases and Ions*; Kauzlarich, S. M., Ed.; VCH Publishers: New York, 1996. (b) Kim, H.; Condron, C. L.; Holm, A. P.; Kauzlarich, S. M. *J. Am. Chem. Soc.* **2000**, *122*, 10720−10721. (c) Holm, A. P.; Olmstead, M. M.; Kauzlarich, S. M. *Inorg. Chem.* **2003**, *42*, 1973−1981.

since examples for a full charge transfer in the sense discussed have been known for a long time.

In 1943, A. Sommer reported on the deposition of cesium onto gold, leading to the formation of an alloy with the simple chemical formula CsAu.[7] Particularly remarkable was a visible change from an opaque gold layer to transparent CsAu, which was found to crystallize with the CsCl structure.[8] On the basis of a series of physical investigations, such as optical absorption spectra, X-ray photoemission spectra, and Mössbauer measurements,[9] CsAu was identified as a semiconductor exhibiting a considerable amount of ionic bonding, and containing gold, with one extra localized electron, as a negatively charged auride ion. Independent experimental evidence confirming this point of view was provided by interdiffusion of the solids CsAu and Cs_2O, leading to the perovskite Cs_3AuO.[10] This experiment has demonstrated the mobility of auride ions as integral entities in the solid state. These results, and further crystal-chemical studies, reveal pronounced parallels to the chemistry of halogenides. Most strikingly, elemental gold disproportionates to Au^+ and Au^- at basic conditions, similar to halogens.[11] All these peculiarities of gold can be explained by its extremely high electron affinity—the highest among all metals (2.31 eV).[12] In full accordance with this fact, the maximum of the relativistic 6s orbital contraction has been reported to occur with gold.[13]

Among the transition metals, platinum has the second highest electron affinity (2.13 eV),[12] in this respect even surpassing all of the chalcogens (2.08 eV for sulfur[12]). The relativistic contraction of its 6s orbital is little smaller than that for gold.[13] As a consequence, one might expect negatively charged platinum anions to exist too. Indeed, we have recently managed to synthesize and characterize dark-red transparent Cs_2Pt.[14] Density functional calculations for Cs_2Pt indicated a band gap of 1.3−1.9 eV, and virtually complete charge separation. Hence, Cs_2Pt was suggested to represent an ionic arrangement consisting of Cs^+ and Pt^{2-}.

However, both Au^- and Pt^{2-} ions are closed shell species, and thus, they would represent trivial borderline cases within the Zintl−Klemm concept. To achieve a less complete charge transfer, we have extended our search for compounds containing platinide ions. Here, we report on a novel BaPt which contains anionic platinum forming homoatomic covalent bonds.

Experimental Details

Synthesis. Materials utilized were Ba (99% Sigma-Aldrich Chemie GmbH, Germany), which was distilled twice at 1100 K in a dynamic vacuum of 10^{-9} bar, and Pt sponge (99.9% Chempur, MaTeck Material-Technologie & Kristalle GmbH, Germany), which was dried and degassed before use at 673 K in a dynamic vacuum of 10^{-9} bar. The elements were weighed out in the ratio 1:1 in an argon-filled glovebox ($[H_2O] < 0.1$ ppm, $[O_2] < 1$ ppm; M. Braun GmbH, Germany), and placed into a tantalum tube, which was sealed under argon with an arc welder. To prevent oxidation, the tantalum tube was encapsulated in a silica jacket under argon. The reaction mixture was heated with a rate of 50 K/h to 1223 K, annealed at this temperature for 2 days, and then cooled to room temperature with a rate of 10 K/h. The product was isolated and handled under strictly inert conditions (Schlenk technique or glovebox).

Table 1. Selected Data Collection and Refinement Parameters for BaPt

space group, Z	$P6_3/mmc$ (No. 194), 2
fw	332.43
lattice parameters (powder data, Å)	$a = 5.057(2)$, $c = 5.420(3)$
volume (Å^3)	120.02(8)
ρ_{calcd} (g·cm^{-3})	9.198
μ (Mo Kα, cm^{-1})	740.6
R1, wR2[a]	0.0297, 0.0787

[a] $R1 = \sum||F_o| - |F_c||/\sum|F_o|$. $wR2 = [\sum w(F_o^2 - F_c^2)^2/\sum w(F_o^2)^2]^{1/2}$. $w^{-1} = [\sigma^2(F_o^2) + (0.0373P)^2 + 3.10P]$ with $P = (1/3)(F_o^2 + 2F_c^2)$.

Table 2. Atomic Coordinates and Anisotropic Displacement Parameters $U_{ij} \times 10^3$ (Å^2) for BaPt[a]

		x	y	z	$U_{11} = U_{22}$	U_{33}	U_{12}
Pt	2*a*	0	0	0	11(1)	20(1)	6(1)
Ba	2*c*	1/3	2/3	1/4	11(1)	25(1)	5(1)

[a] $T = \exp[-2\pi^2(h^2a^{*2}U_{11} + k^2b^{*2}U_{22} + l^2c^{*2}U_{33} + 2hka^*b^*U_{12} + 2hla^*c^*U_{13} + 2klb^*c^*U_{23})]$. $U_{23} = U_{13} = 0$.

Table 3. Selected Bond Distances (Å) and Angles (deg) in BaPt

Pt−Pt	2.710(2) × 2	Ba−Pt−Ba	76.46(2) × 6
Pt−Ba	3.219(1) × 6	Pt−Ba−Pt	49.79(3) × 3
Ba−Pt	3.219(1) × 6	Pt−Ba−Pt	103.54(2) × 6
Ba−Ba	3.984(1) × 6	Pt−Ba−Pt	126.06(1) × 6

Structure Determination. A shiny, black crystal of dimensions 0.08 × 0.08 × 0.12 mm^3 was mounted in a glass capillary inside the glovebox. Data were collected on a SMART-APEX CCD X-ray diffractometer (Bruker) at 293 K with graphite-monochromated Mo Kα radiation. A total of 1800 frames were collected with an exposure time of 30 s/frame. The reflection intensities were integrated with the SAINT[15] subprogram in the SMART[16] software package. The process yielded a total of 1324 reflections, 93 of which were independent and 88 of which had intensities greater than $2\sigma(I)$ ($2\theta_{max} = 61.35°$; $-7 \le h \le +7$, $-7 \le k \le +7$, $-7 \le l \le +7$). Further crystallographic parameters are summarized in Table 1.

The XPREP subprogram of the SHELXTL software package[17] was used to determine the space group. Considering the Laue symmetry and the systematic absences, $P6_3mc$, $P\bar{6}2c$, and $P6_3/mmc$ were suggested as possible space groups. The final choice of $P6_3/mmc$, which has the highest symmetry, was supported by the successful structure determination. Semiempirical absorption correction (SADABS)[18] was applied. The structure was solved by direct methods and refined by full-matrix least squares (R1 = 0.0297, wR2 = 0.0787, and GOF = 1.372 for five parameters refined). The largest residual maximum and minimum in the difference Fourier synthesis were 4.4 and −1.7 e$^-$/Å^3, respectively. Atomic coordinates and anisotropic displacement parameters are listed in Table 2. The anisotropy of the displacement parameters is caused by slight deficiencies in the absorption correction of this heavy-element structure (μ = 740.6 cm^{-1}). Table 3 gives important interatomic distances and bond angles in the structure. More detailed crystallographic information is available in the Supporting Information.

(7) Sommer, A. *Nature* **1943**, *152*, 215.
(8) Kienast, G.; Verma, J.; Klemm, W. *Z. Anorg. Allg. Chem.* **1961**, *310*, 143−169.
(9) (a) Spicer, W. E.; Sommer, A. H.; White, J. G. *Phys. Rev.* **1959**, *115*, 57−62. (b) Wertheim, G. K.; Cohen, R. L.; Crecelius, G.; West, K. W.; Wernick, J. H. *Phys. Rev. B* **1979**, *20*, 860−866.
(10) (a) Feldmann, C.; Jansen, M. *Angew. Chem.* **1993**, *105*, 1107−1108; *Angew. Chem., Int. Ed. Engl.* **1993**, *32*, 1049−1050. (b) Feldmann, C.; Jansen, M. *J. Chem. Soc., Chem. Commun.* **1994**, 1045−1046. (c) Pantelouris, A.; Küper, G.; Hormes, J.; Feldmann, C.; Jansen, M. *J. Am. Chem. Soc.* **1995**, *117*, 11749−11753.
(11) (a) Mudring, A.-V.; Jansen, M. *Angew. Chem.* **2000**, *112*, 3194−3196; *Angew. Chem., Int. Ed.* **2000**, *39*, 3066−3067. (b) Mudring, A.-V.; Nuss, J.; Wedig, U.; Jansen, M. *J. Solid State Chem.* **2000**, *155*, 29−36.
(12) Andersen, T.; Haugen, H. K.; Hotop, H. *J. Phys. Chem. Ref. Data* **1999**, *28*, 1511−1533.
(13) Pyykkö, P.; Desclaux, J. P. *Acc. Chem. Res.* **1979**, *12*, 276−281.
(14) Karpov, A.; Nuss, J.; Wedig, U.; Jansen, M. *Angew. Chem.* **2003**, *115*, 4966−4969; *Angew. Chem., Int. Ed.* **2003**, *42*, 4818−4821.
(15) *SAINT 6.45*; Bruker AXS, Inc.: Madison, WI, 2003.
(16) *SMART 5.630*; Bruker AXS, Inc.: Madison, WI, 1997.
(17) Sheldrick, G. M. *SHELXTL 6.12*; Bruker AXS, Inc.; Madison, WI, 2000.
(18) Sheldrick, G. M. *SADABS 2.10*; Bruker AXS, Inc.: Madison, WI, 2001.

Electron Microscopy. The chemical composition of the compound was investigated using a scanning electron microscope (XL 30 TMP, Philips, Holland; tungsten cathode, 25 kV) equipped with an integrated EDAX−EXD system (S−UTW−Si(Li)−detector).

Powder X-ray Diffraction. To check for phase purity, the compound was examined by X-ray powder diffraction. Powder patterns were collected with a linear position-sensitive detector on a STADI P diffractometer (Stoe & Cie GmbH, Germany; Ge-monochromated Mo $K\alpha_1$ radiation, $2\theta = 4-40°$, step 0.01°). No extra reflections were observed compared to those calculated from atomic coordinates as determined by single-crystal structure analysis using the STOE Win XPOW software.[19] Lattice constants as determined from the powder data are $a = 5.057(2)$ Å, $c = 5.420(3)$ Å, and $c/a = 1.072$.

Differential Thermal Analysis. Differential thermal analysis (DTA) was performed with a computer-controlled thermal analyzer (STA 409, Netzsch GmbH, Germany). A powder sample (19.4 mg) was placed in a tantalum crucible with a lid, heated to 1273 K with a rate of 10 K/min, and then cooled to room temperature with the same rate. The whole process was run under argon.

Band Structure Calculations. DFT band structure calculations with the LDA functional of Von Barth and Hedin[20] were performed using the TB-LMTO-ASA program.[21] Scalar relativistic effects were considered when the partial waves were computed. Details of the computational parameters are given in the Supporting Information. Atomic charges were obtained from a topological analysis of the electron density according to Bader.[22] Bonding properties were investigated both by analyzing the electron localization function (ELF)[23] topologically[24] and by calculating the crystal orbital Hamilton population (COHP).[25] The ELF results from a comparison of the local Pauli repulsion in the compound with that in a uniform electron gas of the respective electron density at a given point. It can take on values between 0 and 1. High ELF values are found in core shells, covalent bonds, and lone pairs. The ELF may be graphically represented either as 2D slices or by isosurfaces of a certain ELF value enveloping regions of higher ELF. The latter are called domains of the ELF that are considered irreducible if they contain only one attractor (maximum). The topological analysis of the ELF leads to basins, which are the spacial regions containing all points whose gradient paths end at the same attractor. Basins may be grouped into basin sets if the ELF at the interconnection point exceeds a certain value. The integration of electron density within basins allows a charge analysis in relation to covalent substructures to be performed. In this work the ELF was calculated from all electrons. The charges within the basins were obtained by integrating the valence electron density. A detailed discussion of the interpretation of the ELF especially in transition-metal compounds has been published by Kohout et al.[26] The ELF proved to be a valuable tool to identify covalent substructures in intermetallic compounds.[27]

Electrical Resistivity. Temperature-dependent resistivity has been obtained for a pressed pellet of BaPt using the van der Pauw method.[28]

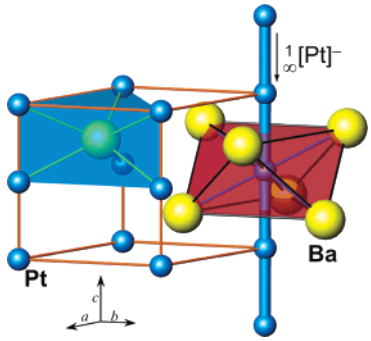

Figure 1. Perspective representation of the crystal structure of BaPt (red, $PtBa_6$ polyhedron; blue, $BaPt_6$ polyhedron; blue thick line, $^1_\infty[Pt]^-$ chains; orange lines, unit cell edges).

BaPt was ground into a powder and subsequently pressed into a 6 mm diameter by 0.55 mm thick pellet. The pellet was then connected to four probes of the resistivity measurement apparatus. A current of 10 mA (Keithley 2400 current source) was applied, and the voltage was measured with a Hewlett-Packard 34420 nanovoltmeter in the temperature range 5−290 K, at 5 K intervals.

Magnetic Measurements. Magnetization was measured using a SQUID magnetometer (MPMS 5.5, Fa., Quantum Design) in the temperature range 5−330 K at $H = 1$, 3, and 5 T, and in addition at lower temperatures (down to 2 K) and a lower magnetic field ($H = 0.0008$ T). The specimen (198.3 mg) was sealed in a silica tube under helium. The raw data were corrected for the holder contribution.

Results and Discussion

BaPt was synthesized by reaction from the elements at 1223 K under argon. According to the powder X-ray diffraction patterns, the product obtained is a single phase. The chemical composition was confirmed by EDX analysis, and no impurity elements were detected. The compound hydrolyzes rapidly when exposed to air. According to DTA measurements, BaPt is thermally stable at least up to 1273 K, which was the maximum temperature investigated.

When the BaPt structure is compared with classical AB structure types, the nickel arsenide structure type may be assigned to BaPt. In a strict sense, in the NiAs structure type, the Ni sites are coordinated octahedrally by six As atoms in the first sphere and by two Ni atoms in the second sphere (coordination number 6 + 2). In contrast, in BaPt, platinum, which occupies the Ni sites, is linearly coordinated by two other platinum atoms that are its nearest neighbors (at a distance of 2.710 Å), and only in the second coordination sphere by six Ba atoms (at a distance of 3.219 Å) in a trigonal antiprismatic manner (coordination number 2 + 6, site symmetry D_{3d}, Figure 1). The most likely driving force for this arrangement is the formation of infinite linear chains of platinum atoms, bonded by homonuclear bonds that are shorter than those in elemental platinum (2.774 Å)[29] and in Krogmann's salt (2.80 Å).[30] In principle, weak metal−metal interactions along the *c* direction are features specific to the NiAs structure, and they are directly reflected by the *c*/*a* ratio. An almost continuous increase of the strength of these bonds from the highest *c*/*a* ratio (2.47) to the smallest one (1.27) has been observed for AB compounds adopting this structure type. According to Laves and Wallbaum,[31] there is a lower limit of the *c*/*a* ratio of $\sqrt{3}/\sqrt{2} = 1.225$;

(19) *STOE Win XPOW 1.06*; Stoe & Cie GmbH: Darmstadt, Germany, 1999.
(20) Von Barth, U.; Hedin, L. *J. Phys. C* **1972**, *5*, 1629−1642.
(21) Tank, R. W.; Jepsen, O.; Burkhardt, A.; Andersen, O. K. *TB-LMTO-ASA 4.7*; Max-Planck-Institut für Festkörperforschung: Stuttgart, Germany, 1998.
(22) Bader, R. F. W. *Atoms in Molecules: a Quantum Theory*; Oxford University Press: Oxford, 1990.
(23) (a) Savin, A.; Becke, A. D.; Flad, J.; Nesper, R.; Preuss, H.; von Schnering, H. G. *Angew. Chem.* **1991**, *103*, 421−424; *Angew. Chem., Int. Ed. Engl.* **1991**, *30*, 409−412. (b) Savin, A.; Jepsen, O.; Flad, J.; Andersen, O. K.; Preuss, H.; von Schnering, H. G. *Angew. Chem.* **1992**, *104*, 186−188; *Angew. Chem., Int. Ed. Engl.* **1992**, *31*, 187−188.
(24) Silvi, B.; Savin, A. *Nature* **1994**, *371*, 683−686.
(25) Dronskowski, R.; Blöchl, P. E. *J. Phys. Chem.* **1993**, *97*, 8617−8624.
(26) Kohout, M.; Wagner, F. R.; Grin, Y. *Theor. Chem. Acc.* **2002**, *108*, 150−156.
(27) (a) Grin, Y.; Wedig, U.; von Schnering, H. G. *Angew. Chem.* **1995**, *107*, 1318−1320; *Angew. Chem., Int. Ed. Engl.* **1995**, *34*, 1204−1206. (b) Grin, Y.; Wedig, U.; Wagner, F.; von Schnering, H. G.; Savin, A. *J. Alloys Compd.* **1997**, *255*, 203−208.
(28) (a) Van der Pauw, L. J. *Philips Res. Rep.* **1958**, *13*, 1−9. (b) Suchet, J. P. In *Electrical Conduction in Solid Materials*; Pamplin, B. R., Gen. Ed.; International Series of Monographs in the Science of the Solid State; Pergamon Press: Oxford, 1975.
(29) Swanson, H. E.; Tatge, E. *J. Res. Nat. Bur. Stand.* **1951**, *46*, 318−327.
(30) (a) Krogmann, K. *Angew. Chem.* **1969**, *81*, 10−17. (b) Krogmann, K.; Hausen, H. D. *Z. Anorg. Allg. Chem.* **1968**, *358*, 67−81.

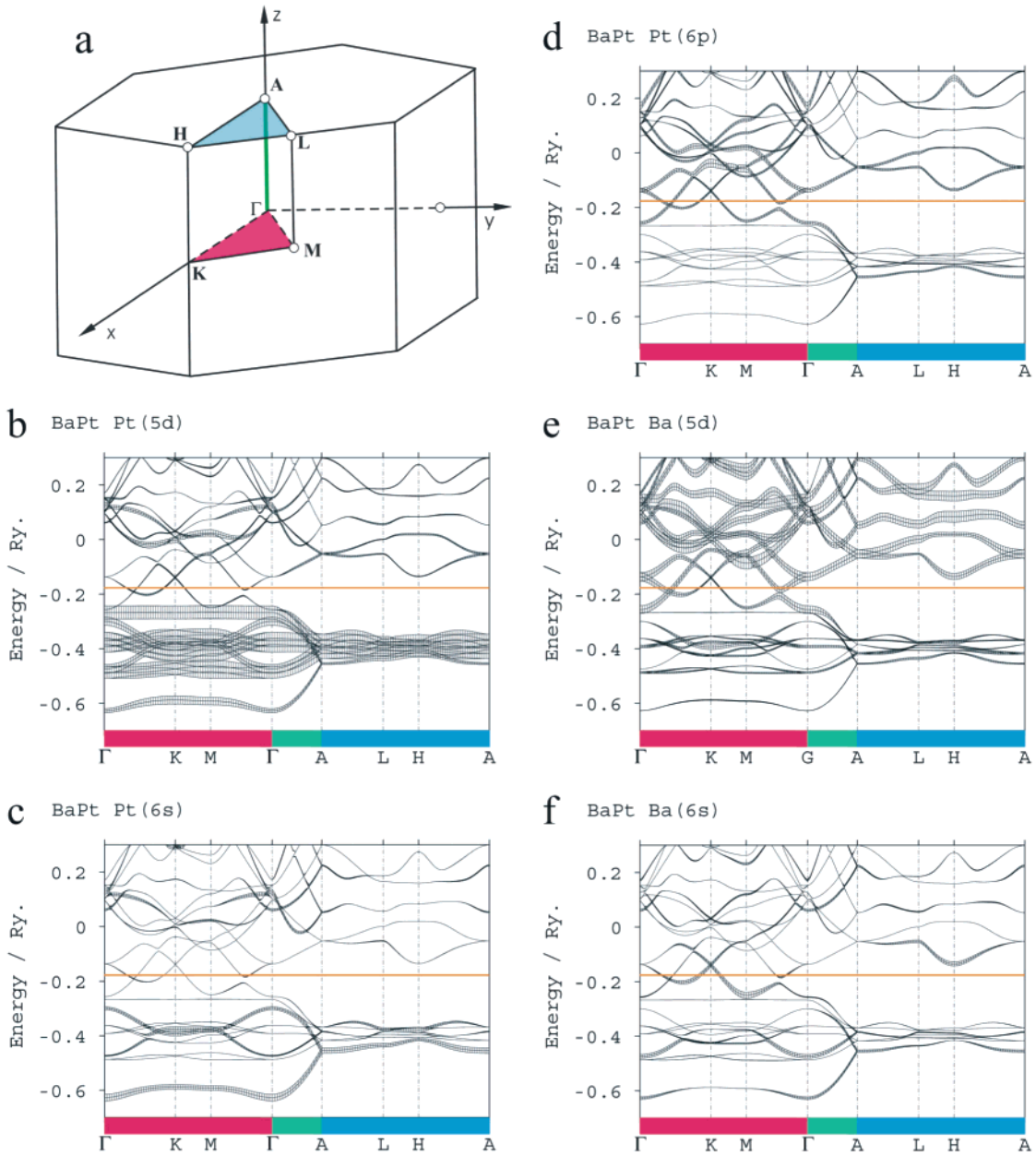

Figure 2. (a) Brillouin zone for a hexagonal crystal with special *k* points as considered in the band structure diagrams. (b−f) TB-LMTO-ASA band structure of BaPt. The widths of the bands show the contribution of different atomic orbitals: (b) Pt 5d, (c) Pt 6s, (d) Pt 6p, (e) Ba 5d (f) Ba 6s. The orange line marks the Fermi level.

however, no reason was given for this assumption. Another theoretical lower limit, $c/a = 0.99 \approx 1$, was discussed by Schönberg,[32] assuming 12-fold contacts of the hexagonally close packed atoms (As, 1/3, 2/3, 1/4). But the same author has stated that this case would never occur. To our knowledge, the lowest c/a ratios for bulk materials under normal pressure have been observed for AuSn ($c/a = 1.278$)[33] and for PtBi ($c/a = 1.272$).[34] It is noteworthy that these values are only slightly lower than the "ideal" c/a ratio of $4/3 = 1.333$, at which Ni atoms in (0,0,0) are coordinated by 6 + 2 atoms at exactly the same distance. As an example of NiAs structures with a high c/a ratio, we mention LaI, where c/a reaches 2.47.[35] The authors have explained this unusually high value by a tendency to maximize the La−La bonds within the *ab* plane. In BaPt, the c/a ratio approaches 1.072, the smallest value ever found for the NiAs structure type. To understand the electronic reasons for this strong contraction, band structure calculations have been performed.

As already found for Cs_2Pt,[14] at the DFT level including relativistic effects, the band with mainly Pt 6s character is situated below the 5d bands, due to the relativistic contraction of the 6s orbital. The 5d bands on their part are well separated from the conduction bands. In addition, the band structures presented in Figure 2 unambiguously reflect the pronounced anisotropic character of the bonding in BaPt. The energies of

(31) Laves, F.; Wallbaum, H. J. *Z. Angew. Mineral.* **1941−42**, *4*, 17−46.
(32) Schönberg, N. *Acta Metall.* **1954**, *2*, 427−432.
(33) Jan, J. P.; Woods, S. B.; Kjekshus, A.; Pearson, W. B. *Can. J. Phys.* **1963**, *41*, 2252−2266.
(34) Zhuravlev, N. N.; Stepanova, A. A. *Sov. Phys. Crystallogr.* **1962**, *7*, 241−242.
(35) Martin, J. D.; Corbett, J. D. *Angew. Chem.* **1995**, *107*, 234−236; *Angew. Chem., Int. Ed. Engl.* **1995**, *34*, 233−235.

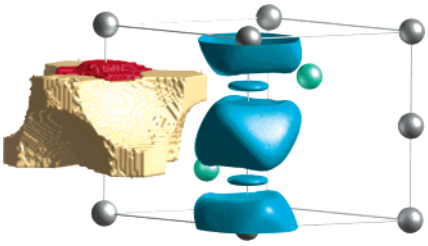

Figure 3. Domains of the ELF (light blue, total ELF $\eta = 0.32$) for a $^1_\infty[Pt]^-$ chain. The reducible domain of the Pt 5d shell as well as the irreducible domain of the Pt−Pt σ bond are shown. The objects on the left side correspond to all basin sets of the ELF attractors included in these domains (yellow, Pt 5d shell; red, Pt−Pt σ bond).

the bands below −0.26 Ry vary but very little if the c^* component of the k points is kept constant. A significant dispersion of bands with Pt $5d_{z^2}$ and Pt 6s contributions occurs only near the Γ point. The dispersion along any k path parallel to c^* in reciprocal space, however, is considerable, especially for the lowest band consisting of Pt 6s with contributions of Pt $5d_{z^2}$. This feature of the band structure is very similar to that of a band of an infinite chain of H atoms, two per unit cell, where the Bloch functions vary from a bonding state at $k = 0$ to a nonbonding state at the boundary of the first Brillouin zone, and points to a strong interaction of the Pt atoms along the c axis of the crystal. The main s character at this lowest band is a first hint of the negative charge state of the Pt atoms, which also results from the topological analysis[22] of the electron density: the Pt basin contains 10.9 electrons.

The interpretation of the band structure given here is confirmed by the investigation of the ELF. In the middle between neighboring Pt atoms within the chains along the c axis ELF attractors ($\eta = 0.35$) appear. The corresponding domains at $\eta = 0.32$ are represented in Figure 3. Their form is typical for a σ-bond, showing covalent interactions within these chains. The integrated electron density within the corresponding basin (red object in Figure 3) obtained from the topological analysis of the ELF amounts to 0.5 electron. The Pt−Pt bonds in the chains exhibit only fractional bond order. Six ELF attractors that can be attributed to the 5d shell of Pt are found at $\eta = 0.64$. Their basins are grouped into two basin sets containing three attractors each at an interconnection value of $\eta = 0.63$. The reducible domain of the Pt 5d shell is also shown in Figure 3. At $\eta = 0.62$ one single basin set is formed (yellow object in Figure 3). This basin set contains 10.6 valence electrons. The integrated valence electron densities within the basins in the Pt chains obtained either from the topological analysis of the total ELF (11.1 electrons) or from the electron density (10.9 electrons) both support the description of the Pt chains along the c axis as $^1_\infty[Pt]^-$.

The covalent interaction within these chains can also be revealed from the COHP curve in Figure 4. Bonding contributions up to −0.4 Ry and some antibonding contributions at about −0.3 Ry, mainly from the $5d_{xz}$ and $5d_{yz}$ orbitals of Pt are integrated up to the Fermi level, to give in total a bonding interaction.

The remaining valence electron has to be associated with the Ba partial structure. This is confirmed by the fat-band representation of the band structure (Figure 2). Contributions to the bands at energies higher than −0.26 Ry, above and below the Fermi level which is located at −0.18 Ry, come mainly from

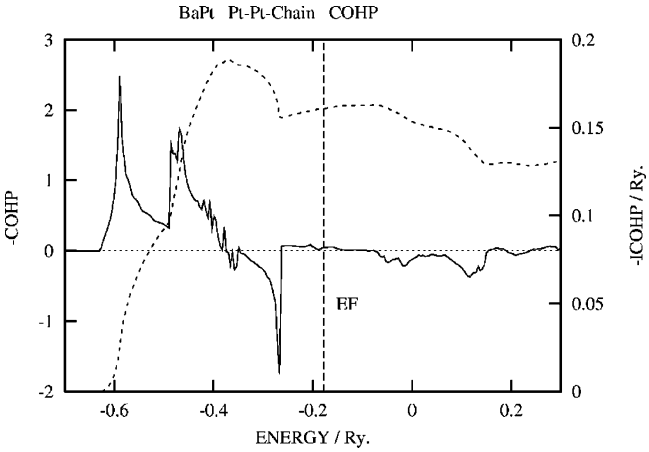

Figure 4. Negative COHP values and their integral of the Pt−Pt bond in the chains parallel to the c axis.

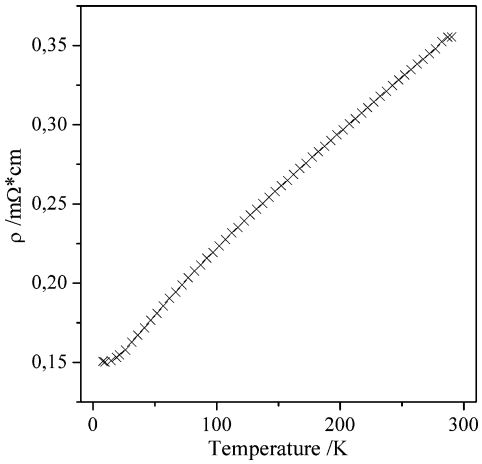

Figure 5. Temperature-dependent resistivity data of BaPt.

orbitals of the Ba atom, especially the 5d orbitals. These dispersive bands cross the Fermi level. In addition, no ELF structures can be found in the Ba partial structure outside the core regions. The remaining valence electron is highly delocalized, which justifies a formal description of the compound as $(Ba^{2+})(^1_\infty[Pt]^-)\cdot e^-$. The band structure shows a gap at the Fermi level at any point in reciprocal space with a nonzero c^* component. The band gap is only closed in the a^*b^* plane of reciprocal space. Thus, BaPt is expected to be a 2D metal exhibiting conductivity parallel to the ab plane.

The specific electrical resistivity increases linearly from 0.15 mΩ·cm at 5 K to 0.35 mΩ·cm at 300 K (Figure 5). This corresponds to a moderate metallic conductor. It should be noted that the resistivity $\rho_{300} = 0.35$ mΩ·cm of BaPt is an order of magnitude higher than that reported for metallic barium ($\rho_{280} = 0.03$ mΩ·cm).[36] The higher value of resistivity might be caused by pores in the pellet as well as different orientations of crystallites. The latter parameter can significantly influence the measured value, where one should keep in mind the 2D conductivity within the Ba layers parallel to the ab plane, predicted by band structure calculations.

Figure 6 shows a temperature dependence of the magnetic susceptibility at fields of 1, 3, and 5 T. The compound exhibits weak diamagnetism. Upon cooling, the susceptibility slowly

(36) Cook, J. G.; Laubitz, M. J. *Can. J. Phys.* **1978**, *56*, 161−174.

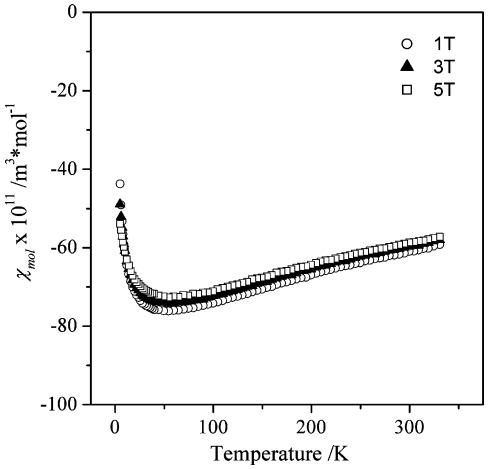

Figure 6. Temperature-dependent magnetic susceptibility data of BaPt.

decreases from -59×10^{-11} m^3/mol at 330 K to -76×10^{-11} m^3/mol at 50 K. At this temperature a minimum occurs. Upon further cooling, the magnetic susceptibility rapidly increases to -44×10^{-11} m^3/mol at 5 K. Four kinds of contributions to magnetization have to be taken into account—the core diamagnetism, the Pauli paramagnetism, the Landau diamagnetism, and the paramagnetic contribution resulting from the positive exchange coupling between conduction d electrons.[37] The first three effects are essentially temperature independent for the range of temperatures considered here. The core diamagnetism for hypothetical $Ba^{2+}Pt^{-}$ can be estimated as $\chi_{dia}(Ba^{2+}Pt^{-}) = \chi_{mol}(Ba^{2+})$[37] $+ \chi_{mol}(Pt^{-}) = (-40 \times 10^{-11}) + (-72 \times 10^{-11}) = -112 \times 10^{-11}$ m^3/mol (the value for $\chi_{mol}(Pt^{-})$ was obtained by a linear fit of the susceptibilities observed for (Pt^{2+}, Pt^{3+}, Pt^{4+})[37] and a linear extrapolation to Pt^{-}). The Pauli paramagnetism and the Landau diamagnetism usually have absolute values an order of magnitude lower than the core contribution. The fourth effect plays an important role for the magnetism of d metals with incompletely filled d shells and is temperature dependent. One of the particularly striking examples is the paramagnetism observed for Pd, reaching $\chi_{mol} = 700 \times 10^{-11}$ m^3/mol at 295 K and 1010×10^{-11} m^3/mol at 80 K.[37] For platinum metal, susceptibilities at temperatures higher than 298 K were reported which are also slightly temperature dependent ($\chi_{mol} = 240 \times 10^{-11}$ m^3/mol at 295 K and 183×10^{-11} m^3/mol at 698 K).[38] The effective magnetic moment of BaPt, $n_{eff} = 797.74[T(\chi_{mol} - \chi_{dia})]^{1/2}$, increases monotonically from 0.04 μ_B (5 K) to 0.34 μ_B (300 K). This corresponds to ~0.0005 (5 K) − 0.03 (300 K) unpaired spins per mole of BaPt assuming the gyromagnetic ratio $g = 2$. The orbital contributions have not been considered. Hence, in the measured temperature range, the Pt 5d shell is almost completely filled. Measurements of the magnetic susceptibility, also conducted at a weak field (0.0008 T), did not reveal any transition to superconductivity down to 2 K. A further detailed electronic and magnetic characterization conducted on a single crystal is required for a better understanding of this compound with such a pronounced anisotropic electronic structure.

Conclusions

As a prominent structural feature, the novel compound BaPt exhibits covalently bonded, infinite linear chains of platinum atoms. Besides the rather short Pt−Pt distances of 2.71 Å found experimentally (in elemental platinum, 2.77 Å), band structure calculations, subsequent topological analyses of both the electron density and the electron localization function, and calculations of the COHPs lend unambiguous support to this view. In particular, the calculations reveal a distinct anisotropy of the bonding in BaPt. Parallel to the a^*b^* planes in reciprocal space, the bands with Pt 6s and Pt 5d orbital character are virtually flat, while they show a strong dispersion parallel to c^*, the direction corresponding to the Pt−Pt bonds. One electron is transferred from barium to platinum, with the remaining valence electron becoming essentially delocalized within the Ba partial structure, resulting in a two-dimensional electronic conductivity parallel to the *ab* plane. The charge distribution and the main structural features are reflected by the formal description $(Ba^{2+})(^{1}_{\infty}[Pt]^{-})\cdot e^{-}$. This scenario, transfer of electronic charge from the electropositive to the electronegative component of an intermetallic phase and formation of covalent bonds among the resulting anions, is strongly reminiscent of the Zintl−Klemm concept. Admittedly, in its canonical meaning, it would not fully apply to BaPt because of an incomplete transfer of the valence electrons of the electropositive metal. However, generalizing this concept, BaPt can be regarded as the first Zintl phase with a transition metal forming a polyanionic component.

Acknowledgment. We gratefully acknowledge C. Muehle for his support of the experimental work, G. Siegle for resistivity measurements, E. Brücher for magnetic measurements, and the Fonds der Chemischen Industrie for continuous financial support.

Supporting Information Available: X-ray crystallographic file (CIF) and a crystallography table, parameters of the TB-LMTO-ASA calculations, the TB-LMTO-ASA band structure of BaPt showing contributions of Pt($5d_{z^2}$), Pt($5d_{x^2-y^2}$), Pt($5d_{xy}$), Pt($5d_{xz}$), Pt($5d_{yz}$), and Ba(6p) atomic orbitals and empty spheres, and temperature-dependent n_{eff} data after correction for the diamagnetic core contribution (PDF). This material is available free of charge via the Internet at http://pubs.acs.org.

JA0401186

(37) Lueken, H. *Magnetochemie*; B. G. Teubner: Stuttgart, Leipzig, Germany, 1999.
(38) Guthrie, A. N.; Bourland, L. T. *Phys. Rev.* **1931**, *37*, 303−308.